

# Observation of multiple van Hove singularities and correlated electronic states in a new topological ferromagnetic kagome metal NdTi<sub>3</sub>Bi<sub>4</sub>

Mazharul Islam Mondal,<sup>1,\*</sup> Anup Pradhan Sakhya,<sup>1,\*</sup> Milo Sprague,<sup>1</sup> Brenden R. Ortiz,<sup>2</sup> Matthew Matzelle,<sup>3</sup> Nathan Valadez,<sup>1</sup> Iftakhar Bin Elius,<sup>1</sup> Barun Ghosh,<sup>3</sup> Arun Bansil,<sup>3</sup> and Madhab Neupane<sup>1,†</sup>

<sup>1</sup>*Department of Physics, University of Central Florida, Orlando, Florida 32816, USA*

<sup>2</sup>*Materials Science and Technology Division, Oak Ridge National Laboratory, Oak Ridge, Tennessee 37830, USA*

<sup>3</sup>*Department of Physics, Northeastern University, Boston, Massachusetts 02115, USA*

(Dated: November 21, 2023)

Kagome materials have attracted enormous research interest recently owing to their diverse topological phases and manifestation of electronic correlation due to their inherent geometric frustration. Here, we report the electronic structure of a new distorted kagome metal NdTi<sub>3</sub>Bi<sub>4</sub> using a combination of angle-resolved photoemission spectroscopy (ARPES) measurements and density functional theory (DFT) calculations. We discover the presence of two flat bands which are found to originate from the kagome structure formed by Ti atoms with major contribution from Ti  $d_{xy}$  and Ti  $d_{x^2-y^2}$  orbitals. We also observed multiple van Hove singularities (VHSs) in its electronic structure, with one VHS lying near the Fermi level ( $E_F$ ). Our results indicate the presence of a surface Dirac cone at the  $\bar{\Gamma}$  point and a linear Dirac-like state at the  $\bar{K}$  point with its Dirac node located very close to the  $E_F$ . Our findings reveal NdTi<sub>3</sub>Bi<sub>4</sub> as a potential material to understand the interplay of topology, magnetism and electron correlation.

## I. INTRODUCTION

Kagome motifs, possessing two-dimensional honeycomb network of corner-sharing triangles have been serving as a useful platform to investigate the complex quantum interactions among frustrated geometry, topological phenomenon, spin, and electronic correlation [1–4]. The kagome motifs exhibit numerous long-range orders with Fermi surface instabilities [5], topological properties and van Hove singularities (VHSs) [3, 4, 6]. The discovery of the AV<sub>3</sub>Sb<sub>5</sub> kagome superconductors have further accelerated research in kagome metals [7–10]. These materials were explored enormously as they exhibit geometric frustration, superconductivity, unconventional charge density wave (CDW) order [11, 12], pair density wave [13], electronic nematicity [14], and giant anomalous Hall effect [15]. A distinct family of Ti based kagome, ATi<sub>3</sub>Bi<sub>5</sub>, was also discovered with potential superconductivity [16, 17], electronic nematicity [18, 19], and nontrivial electronic structure [16, 20].

Apart from these, significant efforts have been focused on magnetic kagome materials such as Fe<sub>3</sub>Sn<sub>2</sub>, FeSn, Co<sub>3</sub>Sn<sub>2</sub>S<sub>2</sub>, Mn<sub>3</sub>Sn, Mn<sub>3</sub>Ge and RMn<sub>6</sub>Sn<sub>6</sub> family ( $R$ = rare earth elements) as they exhibit various exotic phases such as nontrivial Chern gaps, Weyl fermions, and giant anomalous Hall effect [6, 7, 21–36]. Additionally, a new class of materials having the formula AM<sub>3</sub>X<sub>4</sub> (A: Lanthanide, Ca, M:V, Ti, X:Sb, Bi) have been reported [37–39]. YbV<sub>3</sub>Sb<sub>4</sub> is found to be non-magnetic with an absence of distinct thermodynamic transition between 300 K and 60 mK. However when Yb is replaced by Eu,

EuV<sub>3</sub>Sb<sub>4</sub> exhibits a ferromagnetic transition below 32 K [40]. These materials have zig-zag chains of A-site ions and M based distorted kagome sublattices. Further, a large number of Ti based  $LnM_3X_4$  compounds have been synthesized recently [41]. The advantage of this new family of materials is that they provide the possibility of introducing magnetism by selecting a suitable  $Ln$  site element analogous to the  $RMn_6Sn_6$  family. The  $LnM_3X_4$  family thus offers a new setting to explore the interplay between magnetism and inherent geometric frustration. YbTi<sub>3</sub>Bi<sub>4</sub> has been synthesized recently and is found to be non-magnetic [41]. Using ARPES and DFT calculations, YbTi<sub>3</sub>Bi<sub>4</sub> has been reported to host topological Dirac states and correlated states in its electronic structure [42]. NdTi<sub>3</sub>Bi<sub>4</sub>, however is found to be ferromagnetic with its ferromagnetic transition at 9 K [41]. It behaves like a soft ferromagnet with its easy-axis of magnetization lying along the [010] plane. Apart from this report, there is no study on the electronic structure of this material [41].

Here, we have investigated the electronic structure of a new ferromagnetic kagome metal NdTi<sub>3</sub>Bi<sub>4</sub> using angle-resolved photoemission spectroscopy (ARPES) and density-functional theory (DFT) calculations. Using ARPES and DFT calculations, we reveal the presence of two flat bands and multiple VHSs in its electronic band structure. These flat bands originate from Ti kagome lattice and consist predominantly of Ti  $d_{xy}$  and Ti  $d_{x^2-y^2}$  orbitals. In addition, we observe a surface originated Dirac cone at the  $\bar{\Gamma}$  point and a bulk Dirac-like linear band at the  $\bar{K}$  point. The Dirac-like state at the  $\bar{K}$  point is located in the vicinity of the  $E_F$ .

\* These authors contributed equally in this work.

† Corresponding author: [madhab.neupane@ucf.edu](mailto:madhab.neupane@ucf.edu)

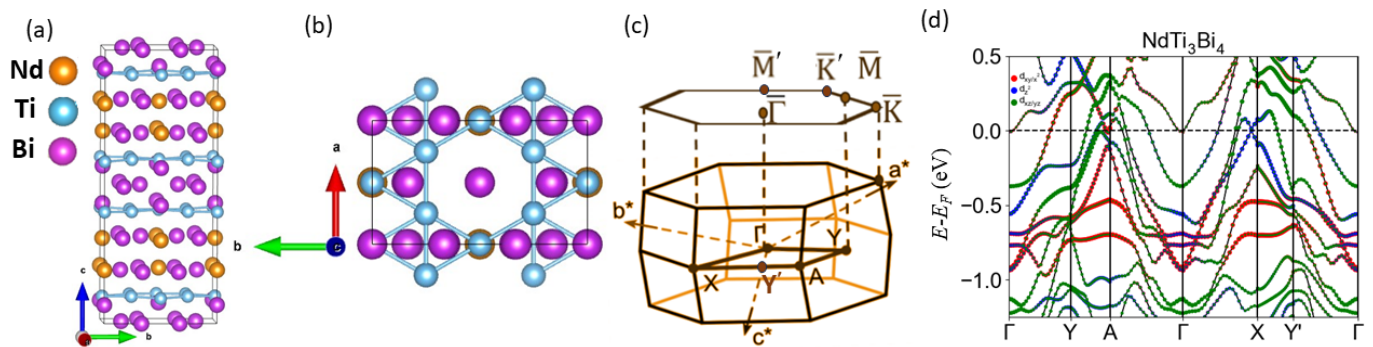


Figure 1. Crystal structure and electronic structure calculation of  $\text{NdTi}_3\text{Bi}_4$ . (a) The  $\text{NdTi}_3\text{Bi}_4$  unit cell with Nd, Ti, and Bi atoms represented as gold, blue, and purple balls, respectively. (b) Unit cell viewed along the  $-c$  vector. The Ti-based kagome structure is highlighted along this orientation. (c) Orthorhombic bulk-Brillouin zone (BZ) with various high-symmetry directions indicated. Above the bulk BZ, the (001) surface-projected pseudo-hexagonal BZ is shown with high-symmetry points indicated. (d) Band dispersion from DFT based calculations with  $d_{xy}/d_{x^2}$ ,  $d_{z^2}$ ,  $d_{xz}/d_{yz}$  orbital projections indicated in red, blue, and green colors respectively.

## II. RESULTS AND DISCUSSION

$\text{NdTi}_3\text{Bi}_4$  crystallizes in the orthorhombic space group  $Fmmm$  (space group No. 69), similar with other reported members of the  $Ln\text{Ti}_3\text{Bi}_4$  family [41], with lattice parameters  $a = 5.89(3)$  Å,  $b = 10.3(3)$  Å,  $c = 24.9(3)$  Å, and  $\alpha = \beta = \gamma = 90^\circ$ . The unit cell consists of Ti kagome layers, shown in blue within Fig 1.(a), separated by alternations of Bi (purple balls) and Bi/Nd (gold) zig-zag layers. A top-down view of the Ti kagome layer along with the Bi intermediate layer is shown in Fig 1.(b) for better visualization of the relevant in-plane lattice characteristics. The in-plane symmetry of  $\text{NdTi}_3\text{Bi}_4$ , along with the other  $Ln\text{Ti}_3\text{Bi}_4$  materials is reduced from the  $C_6$  rotational point group to a  $C_2$  symmetry [41].

Now we move on to discuss the electronic structure. The bulk Brillouin zone (BZ) of  $\text{NdTi}_3\text{Bi}_4$  and its (001) surface projection is shown in Fig. 1(c). High symmetry points are labeled in accordance with the quasi 6-fold rotational symmetry, however the slight  $C_2$  distortion leads us to relabel two  $\bar{M}'$  and  $\bar{K}'$  inequivalent surface high symmetry points. The electronic band dispersions calculated from bulk DFT based first principles calculations, with the inclusion of spin-orbit coupling, are presented in Fig. 1(d). Immediately the metallic nature of this sample is recognized by the high number of bands that cross the Fermi level. Among these are two parabolic bands featuring electron-like curvature at the  $\Gamma$  point, which extends upward to form apparent saddle point van-Hove singularities (VHS) at the  $Y/Y'$  point. The saddle points at  $\bar{Y}$  and  $Y'$  are located at different binding energies. The separate relative positions of these saddle points at the  $Y'$  demonstrates the  $C_6$  symmetry-breaking at play. Similarly, near both the X and A high symmetry points linear Dirac-like crossings are present in close proximity to the Fermi energy, however the crossing near the X point is located exactly at the Fermi energy, whereas the crossing near A is located just below the Fermi energy. We

also note that nondispersive bands are located around  $E - E_F = -0.5$  eV and  $E - E_F = -0.7$  eV.

To corroborate the band-dispersions predicted from DFT calculations, we have performed high-resolution angle-resolved photoemission spectroscopy (ARPES) measurements as presented in Figs. 2-4. In Fig. 2(a), we present the Fermi surface (FS) and constant energy contours (CECs) at various binding energies. Surrounding the  $\bar{\Gamma}$  point are two concentric elliptical pockets with major axes along the  $\bar{\Gamma}-\bar{M}$  (diagonal) direction. The  $\bar{\Gamma}$  pockets are electron-like in dispersion, as indicated by their shrinking volumes over increasing binding energies (going right to left in Fig. 2(a)). Next there exists a large hexagonal pocket with rounded points along the  $\bar{\Gamma} - \bar{K}(\bar{K}')$  direction and flat edges along the  $\bar{M}(\bar{M}') - \bar{K}(\bar{K}')$  direction. Interestingly, there exists a smear of intensity around the  $\bar{M}(\bar{M}')$  point, which appears to protrude from this hexagonal pocket which will be discussed in detail in Fig. 4. Finally, there is a pair of small concentric pockets centered at the  $\bar{K}(\bar{K}')$  point. The inner pocket is nearly point like at the  $\bar{K}(\bar{K}')$  point and the outer pocket features an apparent triangular shape. Both of these pockets increase in volume with increasing binding energy, indicating its hole-like nature.

Fig. 2(b) presents the FS in a wide range. The band dispersion along the  $C_1$  and  $C_2$  directions (see Fig. 2(b)) is presented in Fig. 2(c-e). Along the  $\bar{M}' - \bar{\Gamma} - \bar{M}'$  direction as shown in Fig. 2(c-d) we observed two faint bands surrounding the  $\bar{\Gamma}$  point. These bands become more visible when increasing the photon energy to 50 eV as shown in Fig. 2(d). The innermost band is identified as an electron-like parabolic band with a minimum at about  $E - E_F = -0.3$  eV. The second band corresponding to the outer elliptical pocket is seen to disperse further in binding energy, down to the first flat band. Improved visualization of the bands at the  $\bar{\Gamma}$  point can be achieved by displacing the cut direction by a reciprocal lattice vector

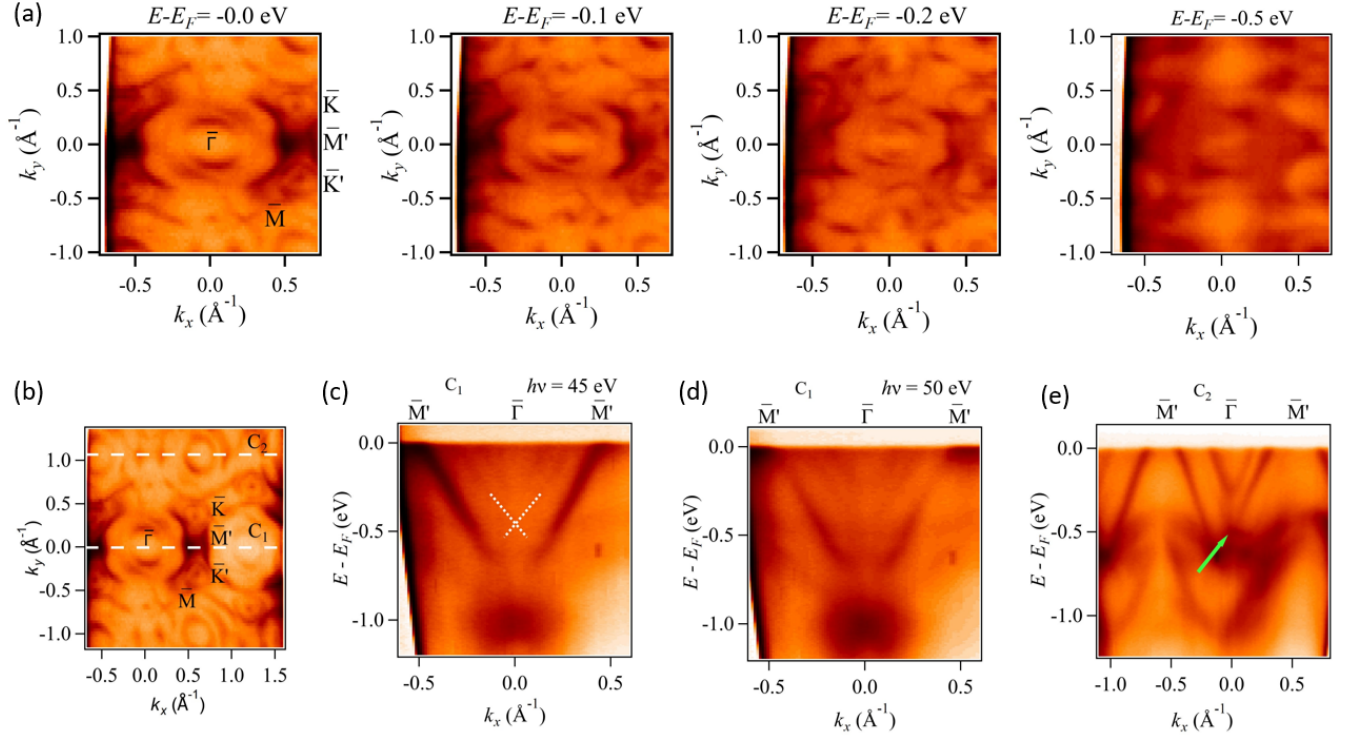


Figure 2. Fermi surface map and constant energy contours of NdTi<sub>3</sub>Bi<sub>4</sub>. (a) The measured Fermi surface and constant energy contours (CECs) with surface-projected high-symmetry points indicated. The CECs are taken at -0.1 eV, -0.2 eV, and -0.5 eV. (b) Wide Fermi surface map with  $\bar{M}' - \bar{\Gamma} - \bar{M}'$  cut shown in the first Brillouin zone (C<sub>1</sub>) and in the second Brillouin zone (C<sub>2</sub>).  $\bar{M}' - \bar{\Gamma} - \bar{M}'$  along C<sub>1</sub> taken using (c) 45 eV and (d) 50 eV incident photons, respectively. The observed linearly dispersing state at  $\bar{\Gamma}$  is outlined using a white-dashed line. (e)  $\bar{M}' - \bar{\Gamma} - \bar{M}'$  cut taken along C<sub>2</sub>.

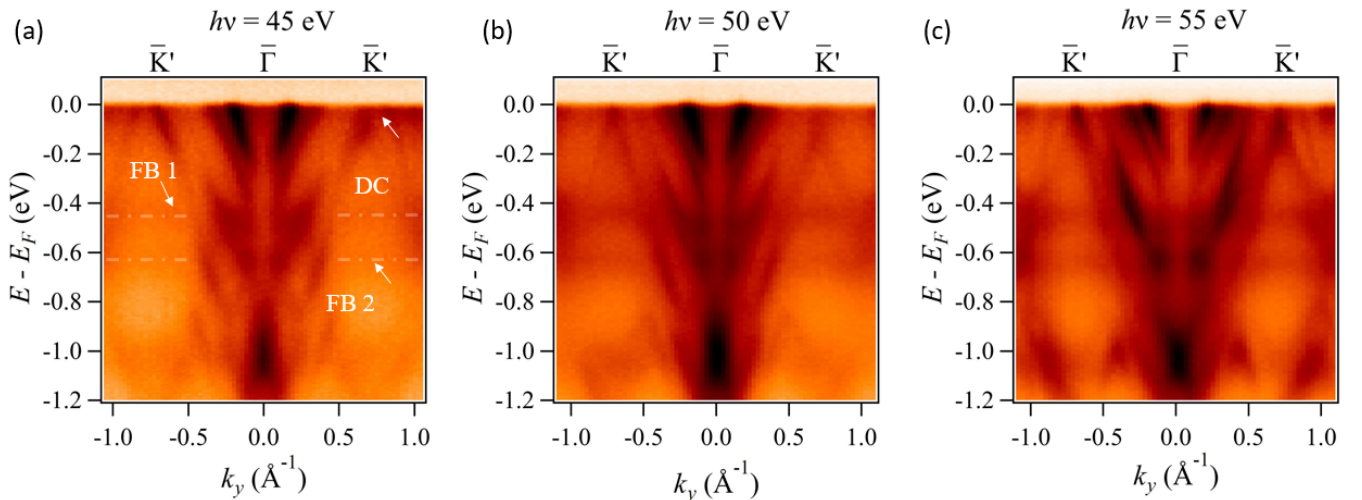


Figure 3. Observation of electronic structure along various high symmetry directions in momentum space. (a) The  $\bar{K}' - \bar{\Gamma} - \bar{K}'$  valence band dispersions are measured using (a) 45 eV, (b) 50 eV, and (c) 55 eV incident photon energies. Attention is drawn to the three relevant features, the linear crossings near  $\bar{K}'$ , and the two flat bands located at  $E - E_F = -0.45$  eV and -0.65 eV through indications with white arrows in panel (a).

to the second BZ, as demonstrated in Fig 2(e) (see green arrow).

Fig. 3 presents the dispersion cut taken along the  $\bar{K}' - \bar{\Gamma} - \bar{K}'$  direction for 45 eV, 50 eV, and 55 eV incident photon energies, respectively. Two flat bands are observed via ARPES dispersion cuts (see white arrows). Linearly dispersing bands are observed surrounding the  $\bar{K}'$  point for each photon energy. Fig 3.(a) taken using 45 eV incident light shows these linearly dispersing states crossing the Fermi energy at two separate momenta. However the dispersion taken using 50 eV photon energy (Fig 3.(b)) shows these states intercepting one another precisely at the Fermi energy. This crossing is shifted slightly downward below the Fermi energy when captured using 55 eV incident light, as observed in Fig 3.(c). These results are identified as linearly dispersing Dirac-like bands expected based on our DFT calculations. In addition to the linearly dispersing states, the  $\bar{K}' - \bar{\Gamma} - \bar{K}'$  cut reveals the presence of two flat bands at about  $E - E_F = -0.45$  eV and  $E - E_F = -0.65$  eV binding energy which is in agreement with our DFT calculations. Orbital-projected DFT calculations as shown in Fig. 1(d) attribute these flat bands to originate from Ti  $d_{xy}$  and Ti  $d_{x^2-y^2}$  orbitals, implicating their origin from the distorted kagome lattice arrangement formed by Ti atoms.

Fig. 4 presents the electronic band dispersion along directions parallel to  $\bar{K}' - \bar{M}' - \bar{K}'$  (panels (b-d)) and  $\bar{M}' - \bar{\Gamma} - \bar{M}'$  (panels (e-g)) directions. The cuts along which the dispersion is shown are indicated in Fig. 4(a), surrounding the  $\bar{M}'$  point. The identification of the saddle point dispersion is done by demonstrating upward curvature along the  $\bar{K}' - \bar{M}' - \bar{K}$  direction and downward curvature along the  $\bar{\Gamma} - \bar{M}' - \bar{\Gamma}$  direction. Cuts 1-3, which correspond to the dispersions presented in Fig. 4(b-d), show an upward curvature to the bands. However when moving through the sequence of cuts the band energy at  $k_y = 0 \text{ \AA}^{-1}$  moves toward the Fermi energy (Fig. 4(a) toward Fig. 4(b)), before reducing in energy again toward Fig. 4(c). Another perspective on the  $\bar{M}'$  saddle point is obtained through perpendicular cuts 4-6. From this angle, the downward dispersion away from the  $\bar{M}'$  point is clearly visualized. The upward dispersion along the perpendicular direction can be understood by observing the steepness of the bands below the Fermi energy. Cut 4 indicates the band maximum is further above the Fermi energy. Moving to cut 5 shows a reduction in the Fermi velocities as the band maximum forming the saddle point disperses closer to the Fermi energy. Continuing beyond the  $\bar{M}'$  shows again an increase in the band maximum in cut 6. Taken together, these six cuts demonstrate the opposite curvature in the dispersions along  $\bar{K}' - \bar{M}' - \bar{K}'$  and  $\bar{M}' - \bar{\Gamma} - \bar{M}'$ , signifying the presence of a saddle-point VHS in close proximity to the Fermi energy. To make the saddle point dispersion most apparent, we have taken the cut along the  $\bar{\Gamma} - \bar{M}' - \bar{K}' - \bar{\Gamma}$  direction for direct com-

parison with the calculated dispersion of Fig. 1(d). Here we find excellent agreement with the DFT results, where the band behavior surrounding the saddle point VHS is in agreement between theory and experiment.

### III. CONCLUSIONS

In summary, we have performed ARPES measurements and DFT calculations for  $\text{NdTi}_3\text{Bi}_4$ , a new distorted ferromagnetic kagome metal. Our ARPES measurements within the paramagnetic phase reveal the presence of multiple VHSs along with two flat bands. These flat bands are found to originate from Ti  $3d_{xy}/3d_{x^2-y^2}$  orbitals, indicating its origin from the destructive interference of Ti kagome motif. We also observe a Dirac cone at the  $\bar{\Gamma}$  point and a bulk linear Dirac-like state near the  $\bar{K}(\bar{K}')$  point. Our discovery of several VHSs and flat bands, which are associated with enhanced electron correlation, along with a non-trivial electronic topology reveal that  $\text{NdTi}_3\text{Bi}_4$  will serve as a promising platform to explore the interplay of magnetism, electronic correlation and topology in this new kagome metal.

*Note added.* Alongside this manuscript, several works were posted on arXiv within a short time period [43–45].

### Methods

#### Experimental and Computational details

$\text{NdTi}_3\text{Bi}_4$  single crystals were grown utilizing a bismuth self-flux method. Nd (Alfa 99.9%), Ti (Alfa 99.9% powder), and Bi (Alfa 99.999% low-oxide shot) elemental reagents were mixed at a ratio of 2:3:12 and placed in 2 mL Canfield crucibles with a catch crucible and a porous frit. The crucibles were airtight under approximately 0.7 atm of argon gas within fused silica ampoules. Each composition was gradually heated to 1050 C at a rate of 200 °C/hr. After reaching 1050 °C, the samples were allowed to thermalize and homogenize for 12-18 hours before cooling to 500 °C at a rate of 2 °C/hr. Excess bismuth was eliminated through centrifugation at 500 °C.

First principles calculations were done using projector augmented-wave pseudopotentials [46] within the Vienna ab initio simulation package (VASP) [47–50]. The strongly constrained and appropriately normed (SCAN) meta-GGA exchange-correlation functional [51] was used. An energy cutoff of 500 eV was adopted for the plane wave basis and the Brillouin zone was sampled by an  $8 \times 8 \times 8$   $\Gamma$  centered grid. The electronic structure was self-consistent until the energy difference between electronic steps was less than  $10^{-6}$  eV. The effects of

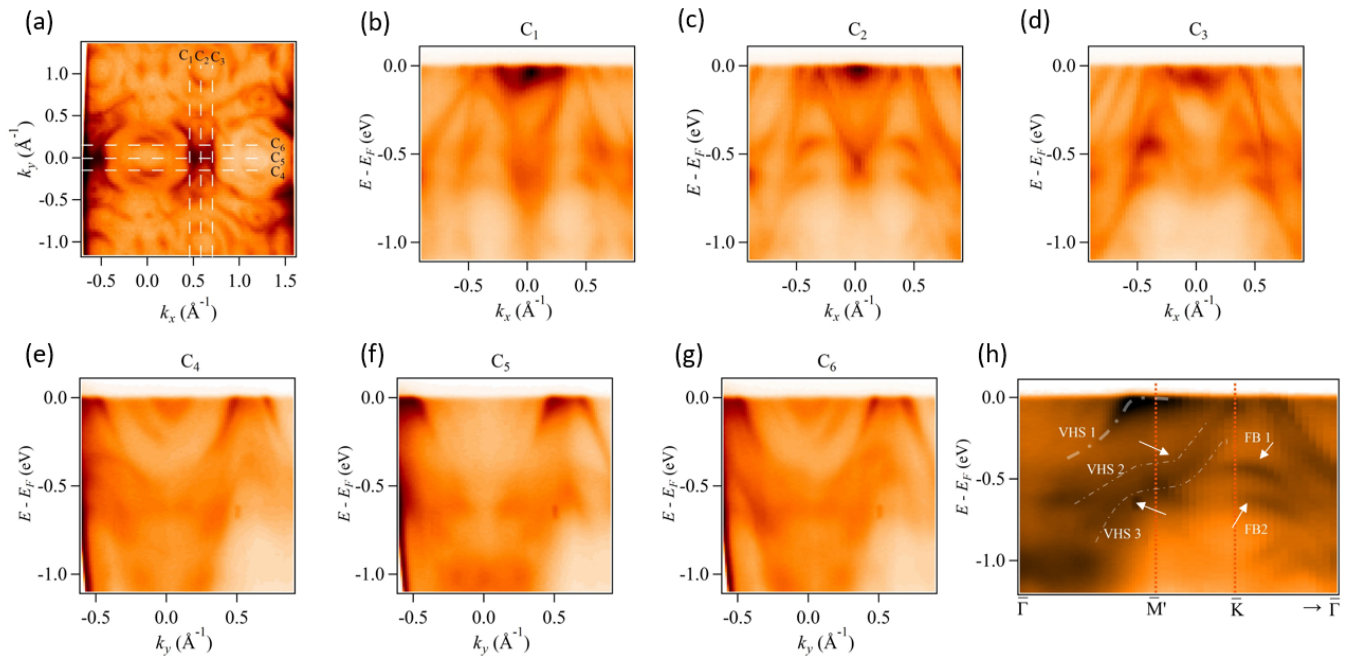


Figure 4. Observation of electronic structure along various high symmetry directions in momentum space. (a) Fermi surface map demonstrating the directions of the cuts presented in panels (b-g). Cuts 1-3, shown in panels (b-d), give the dispersion parallel to, and directly at (c), the  $\bar{K}' - \bar{M}' - \bar{K}$  direction, as indicated by the caption above the panel. Cuts 4-6, shown in panels (e-g), give the dispersion parallel to, and at (f), the  $\bar{M}' - \bar{\Gamma} - \bar{M}'$  direction. (h) The band dispersion along the high-symmetry  $\bar{\Gamma} - \bar{M}' - \bar{K} - \bar{\Gamma}$  path.

spin-orbit coupling are included self-consistently.

### Synchrotron measurements

At ALS, on beamline 10.0.1.1, the electronic structure of NdTi<sub>3</sub>Bi<sub>4</sub> was measured using synchrotron-based ARPES. The measurements were conducted with a Scienta R4000 hemispherical electron analyzer. To ensure a clean surface, the samples were cleaved in an ultra-high vacuum environment (pressure of  $5 \times 10^{-11}$  Torr). The synchrotron measurements had an energy resolution better than 20 meV and an angular resolution finer than  $0.2^\circ$ . The stability of NdTi<sub>3</sub>Bi<sub>4</sub> sample was excellent during the typical 20-hour measurement period with no signs of degradation. The crystals were prepared as small, flat shiny pieces, mounted on copper posts, and ceramic posts were attached on top using silver epoxy. These prepared samples were then loaded into the measurement setup for studying the electronic structure.

### IV. ACKNOWLEDGEMENT

M.N. acknowledges support from the Air Force Office of Scientific Research MURI (Grant No. FA9550-20-1-0322) and the National Science Foundation (NSF) CAREER award DMR1847962. Work performed by B.R.O.

is sponsored by the Laboratory Directed Research and Development Program of Oak Ridge National Laboratory, managed by UT-Battelle, LLC, for the US Department of Energy. The work at Northeastern University was supported by the Air Force Office of Scientific Research under Award No. FA9550-20-1-0322, and it benefited from the computational resources of Northeastern University's Advanced Scientific Computation Center (ASCC) and the Discovery Cluster. This research used resources of the Advanced Light Source, a U.S. Department of Energy Office of Science User Facility, under Contract No. DE-AC02-05CH11231. We thank Sung-Kwan Mo for beamline assistance at the Advanced Light Source (ALS), Lawrence Berkeley National Laboratory.

### REFERENCES

- [1] J. Strečka, L. Čanová, M. Jaščur, and M. Hagiwara, *Phys. Rev. B* **78**, 024427 (2008).
- [2] H. M. Guo and M. Franz, *Phys. Rev. B* **80**, 113102 (2009).
- [3] J.-X. Yin, B. Lian, and M. Z. Hasan, *Nature* **612**, 647 (2022).
- [4] M. Kang, S. Fang, L. Ye, H. C. Po, J. Denlinger, C. Jozwiak, A. Bostwick, E. Rotenberg, E. Kaxiras, J. G. Checkelsky, and R. Comin, *Nat. Commun.* **11**, 4004 (2020).
- [5] W.-S. Wang, Z.-Z. Li, Y.-Y. Xiang, and Q.-H. Wang, *Phys. Rev. B* **87**, 115135 (2013).

- [6] L. Ye, M. Kang, J. Liu, F. von Cube, C. R. Wicker, T. Suzuki, C. Jozwiak, A. Bostwick, E. Rotenberg, D. C. Bell, L. Fu, R. Comin, and J. G. Checkelsky, *Nature* **555**, 638 (2018).
- [7] B. R. Ortiz, L. C. Gomes, J. R. Morey, M. Winiarski, M. Bordelon, J. S. Mangum, I. W. H. Oswald, J. A. Rodriguez-Rivera, J. R. Neilson, S. D. Wilson, E. Ertekin, T. M. McQueen, and E. S. Toberer, *Phys. Rev. Mater.* **3**, 094407 (2019).
- [8] B. R. Ortiz, S. M. L. Teicher, Y. Hu, J. L. Zuo, P. M. Sarte, E. C. Schueller, A. M. M. Abeykoon, M. J. Krogstad, S. Rosenkranz, R. Osborn, R. Seshadri, L. Balents, J. He, and S. D. Wilson, *Phys. Rev. Lett.* **125**, 247002 (2020).
- [9] B. R. Ortiz, P. M. Sarte, E. M. Kenney, M. J. Graf, S. M. L. Teicher, R. Seshadri, and S. D. Wilson, *Phys. Rev. Mater.* **5**, 034801 (2021).
- [10] Q. Yin, Z. Tu, C. Gong, Y. Fu, S. Yan, and H. Lei, *Chin. Phys. Lett.* **38**, 037403 (2021).
- [11] H. Li, T. Zhang, T. Yilmaz, Y. Pai, C. Marvinney, A. Said, Q. Yin, C. Gong, Z. Tu, and E. Vescovo, *Phys. Rev. X* **11**, 031050 (2021).
- [12] Z. Liang, X. Hou, F. Zhang, W. Ma, P. Wu, Z. Zhang, F. Yu, J. J. Ying, K. Jiang, L. Shan, Z. Wang, and X. H. Chen, *Phys. Rev. X* **11**, 031026 (2021).
- [13] H. Chen, H. Yang, B. Hu, Z. Zhao, J. Yuan, Y. Xing, G. Qian, Z. Huang, G. Li, Y. Ye, S. Ma, S. Ni, H. Zhang, Q. Yin, C. Gong, Z. Tu, H. Lei, H. Tan, S. Zhou, C. Shen, X. Dong, B. Yan, Z. Wang, and H.-J. Gao, *Nature* **599**, 222 (2021).
- [14] L. Nie, K. Sun, W. Ma, D. Song, L. Zheng, Z. Liang, P. Wu, F. Yu, J. Li, and M. Shan, *Nature* **604**, 59 (2022).
- [15] S.-Y. Yang, Y. Wang, B. R. Ortiz, D. Liu, J. Gayles, E. Derunova, R. Gonzalez-Hernandez, L. Šmejkal, Y. Chen, S. S. P. Parkin, S. D. Wilson, E. S. Toberer, T. McQueen, and M. N. Ali, *Sci. Adv.* **6**, eabb6003 (2020).
- [16] H. Yang, Z. Zhao, X.-W. Yi, J. Liu, J.-Y. You, Y. Zhang, H. Guo, X. Lin, C. Shen, and H. Chen, *arXiv preprint arXiv:2209.03840* (2022).
- [17] X.-W. Yi, X.-Y. Ma, Z. Zhang, Z.-W. Liao, J.-Y. You, and G. Su, *Phys. Rev. B* **106**, L220505 (2022).
- [18] H. Yang, Y. Ye, Z. Zhao, J. Liu, X.-W. Yi, Y. Zhang, J. Shi, J.-Y. You, Z. Huang, and B. Wang, *arXiv preprint arXiv:2211.12264* (2022).
- [19] H. Li, S. Cheng, B. R. Ortiz, H. Tan, D. Werhahn, K. Zeng, D. Johrendt, B. Yan, Z. Wang, and S. D. Wilson, *Nat. Phys.*, **1** (2023).
- [20] D. Werhahn, B. R. Ortiz, A. K. Hay, S. D. Wilson, R. Seshadri, and D. Johrendt, *Zeitschrift für Naturforschung B* **77**, 757 (2022).
- [21] J.-X. Yin, W. Ma, T. A. Cochran, X. Xu, S. S. Zhang, H.-J. Tien, N. Shumiya, G. Cheng, K. Jiang, B. Lian, Z. Song, G. Chang, I. Belopolski, D. Multer, M. Litskevich, Z.-J. Cheng, X. P. Yang, B. Swidler, H. Zhou, H. Lin, T. Neupert, Z. Wang, N. Yao, T.-R. Chang, S. Jia, and M. Zahid Hasan, *Nature* **583**, 533 (2020).
- [22] E. Liu, Y. Sun, N. Kumar, L. Muechler, A. Sun, L. Jiao, S.-Y. Yang, D. Liu, A. Liang, Q. Xu, J. Kroder, V. Süß, H. Borrmann, C. Shekhar, Z. Wang, C. Xi, W. Wang, W. Schnelle, S. Wirth, Y. Chen, S. T. B. Goennenwein, and C. Felser, *Nat. Phys.* **14**, 1125 (2018).
- [23] T. Asaba, S. M. Thomas, M. Curtis, J. D. Thompson, E. D. Bauer, and F. Ronning, *Phys. Rev. B* **101**, 174415 (2020).
- [24] N. J. Ghimire, R. L. Dally, L. Poudel, D. C. Jones, D. Michel, N. T. Magar, M. Bleuel, M. A. McGuire, J. S. Jiang, J. F. Mitchell, J. W. Lynn, and I. I. Mazin, *Sci. Adv.* **6**, eabe2680 (2020).
- [25] J.-X. Yin, W. Ma, T. A. Cochran, X. Xu, S. S. Zhang, H.-J. Tien, N. Shumiya, G. Cheng, K. Jiang, B. Lian, Z. Song, G. Chang, I. Belopolski, D. Multer, M. Litskevich, Z.-J. Cheng, X. P. Yang, B. Swidler, H. Zhou, H. Lin, T. Neupert, Z. Wang, N. Yao, T.-R. Chang, S. Jia, and M. Zahid Hasan, *Nature* **583**, 533 (2020).
- [26] W. Ma, X. Xu, J.-X. Yin, H. Yang, H. Zhou, Z.-J. Cheng, Y. Huang, Z. Qu, F. Wang, M. Z. Hasan, and S. Jia, *Phys. Rev. Lett.* **126**, 246602 (2021).
- [27] L. Gao, S. Shen, Q. Wang, W. Shi, Y. Zhao, C. Li, W. Cao, C. Pei, J.-Y. Ge, G. Li, J. Li, Y. Chen, S. Yan, and Y. Qi, *Appl. Phys. Lett.* **119** (2021).
- [28] W. Ma, X. Xu, Z. Wang, H. Zhou, M. Marshall, Z. Qu, W. Xie, and S. Jia, *Phys. Rev. B* **103**, 235109 (2021).
- [29] M. Li, Q. Wang, G. Wang, Z. Yuan, W. Song, R. Lou, Z. Liu, Y. Huang, Z. Liu, H. Lei, Z. Yin, and S. Wang, *Nat. Commun.* **12**, 3129 (2021).
- [30] G. Dhakal, F. Cheenicode Kabeer, A. K. Pathak, F. Kabir, N. Poudel, R. Filippone, J. Casey, A. P. Sakhya, S. Regmi, C. Sims, K. Dimitri, P. Manfrinetti, K. Gofryk, P. M. Oppeneer, and M. Neupane, *Phys. Rev. B* **104**, L161115 (2021).
- [31] Q. Wang, K. J. Neubauer, C. Duan, Q. Yin, S. Fujitsu, H. Hosono, F. Ye, R. Zhang, S. Chi, K. Krycka, H. Lei, and P. Dai, *Phys. Rev. B* **103**, 014416 (2021).
- [32] H. Zeng, G. Yu, X. Luo, C. Chen, C. Fang, S. Ma, Z. Mo, J. Shen, M. Yuan, and Z. Zhong, *J. Alloys Compd.* **899**, 163356 (2022).
- [33] X. Gu, C. Chen, W. S. Wei, L. L. Gao, J. Y. Liu, X. Du, D. Pei, J. S. Zhou, R. Z. Xu, Z. X. Yin, W. X. Zhao, Y. D. Li, C. Jozwiak, A. Bostwick, E. Rotenberg, D. Backes, L. S. I. Veiga, S. Dhesi, T. Hesjedal, G. van der Laan, H. F. Du, W. J. Jiang, Y. P. Qi, G. Li, W. J. Shi, Z. K. Liu, Y. L. Chen, and L. X. Yang, *Phys. Rev. B* **105**, 155108 (2022).
- [34] F. Kabir, R. Filippone, G. Dhakal, Y. Lee, N. Poudel, J. Casey, A. P. Sakhya, S. Regmi, R. Smith, P. Manfrinetti, L. Ke, K. Gofryk, M. Neupane, and A. K. Pathak, *Phys. Rev. Mater.* **6**, 064404 (2022).
- [35] R. S. Li, T. Zhang, W. Ma, S. X. Xu, Q. Wu, L. Yue, S. J. Zhang, Q. M. Liu, Z. X. Wang, T. C. Hu, X. Y. Zhou, D. Wu, T. Dong, S. Jia, H. Weng, and N. L. Wang, *Phys. Rev. B* **107**, 045115 (2023).
- [36] B. Lv, R. Zhong, X. Luo, S. Ma, C. Chen, S. Wang, Q. Luo, F. Gao, C. Fang, W. Ren, and Z. Zhong, *J. Alloys Compd.* **957**, 170356 (2023).
- [37] Ortiz, B. R., et al. YbV<sub>3</sub>Sb<sub>4</sub> and EuV<sub>3</sub>Sb<sub>4</sub> vanadium-based kagome metals with Yb<sup>2+</sup> and Eu<sup>2+</sup> zigzag chains. *Phys. Rev. Mater.* **7**, 064201 (2023).
- [38] A. Ovchinnikov and S. Bobev, *Eur. J. Inorg. Chem.* **2018**, 1266 (2018).
- [39] A. Ovchinnikov and S. Bobev, *Inorg. Chem.* **59**, 3459 (2020).
- [40] B. R. Ortiz, G. Pokharel, M. Gundayao, H. Li, F. Kaboudvand, L. Kautzsch, S. Sarker, J. P. Ruff, T. Hogan, and S. J. G. Alvarado, *Phys. Rev. Mater.* **7**, 064201 (2023).
- [41] B. R. Ortiz, H. Miao, F. Yang, E. M. Clements, D. S. Parker, J. Yan, A. F. May, and M. A. McGuire, *arXiv:2308.16138v1*, (2023).

- [42] A. P. Sakhya, B. R. Ortiz, B. Ghosh, M. Sprague, M. I. Mondal, M. Matzelle, I. B. Elius, N. Valadez, D. G. Mandrus, and A. Bansil, [arXiv preprint arXiv:2309.01176 \(2023\)](#).
- [43] L. Chen, Y. Zhou, H. Zhang, X. Ji, K. Liao, Y. Ji, Y. Li, Z. Guo, X. Shen, and R. Yu, [arXiv preprint arXiv:2307.02942, \(2023\)](#).
- [44] J. Guo, L. Zhou, J. Ding, G. Qu, Z. Liu, Y. Du, H. Zhang, J. Li, Y. Zhang, and F. Zhou, [arXiv preprint arXiv:2308.14509, \(2023\)](#).
- [45] Y. Hu, C. Le, L. Chen, H. Deng, Y. Zhou, N. C. Plumb, M. Radovic, R. Thomale, A. P. Schnyder, and J.-X. Yin, [arXiv preprint arXiv:2311.07747 \(2023\)](#).
- [46] G. Kresse and D. Joubert, *Phys. Rev. B* **59**, 1758 (1999).
- [47] G. Kresse and J. Hafner, *Phys. Rev. B* **47**, 558 (1993).
- [48] G. Kresse and J. Hafner, *Phys. Rev. B* **49**, 14251 (1994).
- [49] G. Kresse and J. Furthmüller, *Comput. Mater. Sci.* **6**, 15 (1996).
- [50] G. Kresse and J. Furthmüller, *Phys. Rev. B* **54**, 11169 (1996).
- [51] J. Sun, A. Ruzsinszky, and J. P. Perdew, *Phys. Rev. Lett.* **115**, 036402 (2015).